PARTIAL REFLECTIONS OF RADIO WAVES FROM THE LOWER IONOSPHERE

by Denis J. Connolly and B. Samuel Tanenbaum

Lewis Research Center
Cleveland, Ohio 44135

NATIONAL AERONAUTICS AND SPACE ADMINISTRATION • WASHINGTON, D. C. • APRIL 1972

1. Report No.	2. Government Accession No.	3. Recipient's Catalog No.
NASA TN D-6742		

4. Title and Subtitle	5. Report Date
PARTIAL REFLECTIONS OF RADIO WAVES FROM THE LOWER IONOSPHERE	April 1972
	6. Performing Organization Code

7. Author(s)	8. Performing Organization Report No.
Denis J. Connolly, Lewis Research Center; and B. Samuel Tanenbaum, Case Western Reserve University, Cleveland, Ohio	E-6701
	10. Work Unit No. 112-02

9. Performing Organization Name and Address	11. Contract or Grant No.
Lewis Research Center National Aeronautics and Space Administration Cleveland, Ohio 44135	
	13. Type of Report and Period Covered: Technical Note

12. Sponsoring Agency Name and Address	14. Sponsoring Agency Code
National Aeronautics and Space Administration Washington, D.C. 20546	

15. Supplementary Notes

16. Abstract

The addition of phase difference measurements to partial reflection experiments is discussed, and some advantages of measuring electron density this way are pointed out. The additional information obtained reduces the requirement for an accurate predetermination of collision frequency. Calculations are also made to estimate the errors expected in partial-reflection experiments due to the assumption of Fresnel reflection and to the neglect of coupling between modes. In both cases, the errors are found to be of the same order as known errors in the measurements due to current instrumental limitations.

17. Key Words (Suggested by Author(s))	18. Distribution Statement
Partial reflections D region Differential phase Mode coupling	Unclassified - unlimited

19. Security Classif. (of this report)	20. Security Classif. (of this page)	21. No. of Pages	22. Price*
Unclassified	Unclassified	49	$3.00

* For sale by the National Technical Information Service, Springfield, Virginia 22151

PARTIAL REFLECTIONS OF RADIO WAVES FROM THE LOWER IONOSPHERE

by Denis J. Connolly and B. Samuel Tanenbaum*

Lewis Research Center

SUMMARY

The addition of phase difference measurements to lower ionosphere (50 to 100 km) partial reflection experiments is discussed and some advantages in measuring electron density this way are pointed out. In particular, the determination of electron density through phase difference measurements is less sensitive to errors in the assumed collision frequency profile. Both electron density and collision frequency can be determined through measurements of differential absorption and phase shift.

In partial reflection experiments, the reflections are usually treated as simple Fresnel reflections from a plane interface. A more reasonable one-dimensional model for the reflecting layers is an Epstein profile. It is shown that the ratio of reflection coefficients, as calculated for this type of profile, can differ appreciably from the result given by Fresnel reflection.

The effect of mode coupling in the reflection process is also considered. It is found to be a fairly small effect which increases in importance with increasing electron density. Mode coupling could contribute appreciable errors in differential absorption experiments if the electron density approaches 10^4 per cubic centimeter.

INTRODUCTION

The differential absorption of the two magnetoionic modes has been used to study the lower ionosphere since 1953 (ref. 1). Radio waves in the frequency range from about 2 to 6 megahertz (usually close to 2.5 MHz) are transmitted up into the atmosphere. Ionization irregularities in the 50- to 100-kilometer height range give rise to partial reflections in this frequency range on a fairly regular basis (refs. 2 to 4). The reflected waves are resolved into ordinary and extraordinary components by the receiving equipment used. The amplitudes of the two components are recorded as functions

*Professor of Engineering, Case Western Reserve University, Cleveland, Ohio.

of apparent height. One can then calculate an electron density profile by using an assumed model for the reflection mechanism, an assumed collision frequency profile, and the experimental curve of amplitude ratio against height. The reasonableness of the assumptions used is discussed in reference 5. Some of these assumptions will be considered in greater detail in this report.

It has been pointed out in reference 6 that the phase angle between the two modes would also provide useful information. A sufficiently accurate measurement of both the differential absorption and differential phase shift would determine both the electron density and collision frequency profiles. The value of the technique has been further discussed in references 7 to 9. Reference 10 describes a method whereby the phase difference is obtained indirectly through measurements of the power received by linearly polarized antennas with different directions of polarization. The method presented in reference 10 appears to be strictly applicable only when the quasi-longitudinal approximation is valid (the two wave polarizations are taken as $\pm i$ in eq. (9) of ref. 10). In the HF band (2 to 6 MHz), the validity of this approximation varies widely with magnetic latitude. A direct measurement of phase difference would not have this limitation.

The differential phase and differential absorption techniques are outlined in the following sections. The theoretical basis of the two techniques is briefly described. The reflection mechanism is then discussed from the simple Fresnel reflection viewpoint. Most of this report concerns corrections to this simple approach.

Recent discussions have centered on the use of the phase-difference method to study the reflection producing irregularities. In this report, the dependence of differential absorption and differential phase shift on the electron density and collision frequency in the medium is discussed. It is shown, by a fairly simple theoretical discussion, that the phase difference method has a number of important potential advantages over the differential absorption method.

The reflection process is also examined in some detail. First, the magnitude of errors to be expected if the vertical scale of the irregularities is not small compared to a wave length is calculated by assuming an Epstein profile. Then, the possibility of errors due to mode coupling in the reflection process is considered.

All the scattering calculations of this report treat steady-state reflections from a single horizontally uniform scattering region. In an experimental situation, the radar system transmits pulses and accepts returns from a large volume of space. The plasma properties in this volume vary from point to point, as well as with time. Therefore, some effects of finite pulses on a partial reflection experiment are discussed. Also discussed, in a qualitative way, are the respects in which the theory might be modified to account for more realistic reflecting irregularities. Appendix A contains a list of the symbols used in this report. Appendixes B and C provide background information and calculations referred to in the text.

OUTLINE OF PARTIAL REFLECTION METHOD

Basis of Differential Absorption and Differential Phase Techniques

In the partial reflection experiments, pulsed radio waves are transmitted upwards into the ionosphere. Both magnetoionic modes are transmitted either simultaneously or on alternate pulses. Small amounts of the power in each mode are reflected from irregularities in the lower ionosphere. The electric field reflection coefficients referred to the ground are (ref. 11, p. 136)

$$A_{o,\,e} = R_{o,\,e} \exp\left(-\frac{2i\omega}{c}\int_0^h n_{o,\,e}\,dz\right) \tag{1}$$

where R_o and R_e are the reflection coefficients for ordinary and extraordinary waves referred to the height of reflection h, and n_o and n_e are the complex indices of refraction for the ordinary and extraordinary waves. Then

$$\frac{A_o}{A_e} = \frac{R_o}{R_e} \exp\left[-\frac{2i\omega}{c}\int_0^h (n_o - n_e)dz\right] \tag{2}$$

and it follows that

$$\frac{d}{dh} \ln \frac{A_o R_e}{A_e R_o} = -\frac{2i\omega}{c}(n_o - n_e) \tag{3}$$

If the real and imaginary parts of equation (3) are considered separately, then

$$\frac{d}{dh} \ln \left|\frac{A_o R_e}{A_e R_o}\right| = \frac{2\omega}{c} \mathrm{Im}(n_o - n_e) \tag{4}$$

$$\frac{d}{dh} \mathrm{phase}\left[\frac{A_o R_e}{A_e R_o}\right] = -\frac{2\omega}{c} R_e(n_o - n_e) \tag{5}$$

Equation (4) is the relation used in the differential absorption experiments. For this equation, $|A_o/A_e|$ is supplied by experiment, and $|R_e/R_o|$ is inferred from the assumed reflection mechanism and the assumed collision frequency profile. The result is a value

for $\mathrm{Im}(n_o - n_e)$ which, again with the use of the assumed collision frequency profile, determines an electron density profile.

A similar procedure can be followed with equation (5). The phase of A_o/A_e can be determined by experiment. The phase of R_e/R_o is determined, along with the amplitude, by the assumed reflection mechanism. The result is a profile for the real part of $(n_o - n_e)$ as a function of height.

From the real and imaginary parts of $(n_o - n_e)$ we can, in principle, determine both the electron density and collision frequency at height h. Some of the practical limitations are discussed in other parts of this report.

The Reflection Mechanism

The exact nature of the irregularities which give rise to partial reflections is unknown. They are thought to be horizontally stratified, with transverse dimensions at least comparable to the central Fresnel zone (ref. 12), which is typically a few kilometers. The irregularities involve significant changes in electron density over vertical distances of the order of 100 meters or less (ref. 13). The collision frequency is probably constant on this length scale (ref. 5).

The reflection coefficients can be calculated by using the Appleton-Hartree equation for index of refraction

$$n_{o,e}^2 = 1 - \frac{X}{1 - iZ - \frac{Y_T^2}{2(1 - X - iZ)} \pm \left[\frac{Y_T^4}{4(1 - X - iZ)^2} + Y_L^2\right]^{1/2}} \tag{6}$$

$$n_{o,e}^2 = 1 - \frac{X}{W_{o,e}} \tag{7}$$

Equation (6) uses the standard notation (ref. 11). The quantities W_o and W_e in equation (7) are treated as constant through an irregularity since they depend only weakly on X when $X \ll 1$. (At an electron density of 10^4 per cm^3 and a frequency of 2.5 MHz, $X \approx 0.1$.) The more exact magnetoionic formula from reference 14 is often used in place of equation (6). It can also be written in the same form as equation (7), with $W_{o,e}$ only weakly dependent on X.

The irregularities in index of refraction are therefore given by

$$\Delta n_{o,e} \approx \frac{1}{2}\Delta\left(1 - \frac{X}{W_{o,e}}\right) \approx -\frac{\Delta X}{2W_{o,e}} \tag{8}$$

Consequently,

$$\frac{\Delta n_o}{\Delta n_e} \approx \frac{W_e}{W_o} \tag{9}$$

Equation (9) is used in conjunction with the Fresnel reflection formula for reflection coefficient (assuming vertical incidence)

$$R_{o,e} = \frac{\Delta n_{o,e}}{2n_{o,e} + \Delta n_{o,e}} \approx \frac{\Delta n_{o,e}}{2} \tag{10}$$

or

$$\frac{R_o}{R_e} \approx \frac{\Delta n_o}{\Delta n_e} \approx \frac{W_e}{W_o} = \frac{1 - n_o^2}{1 - n_e^2} \tag{11}$$

If the irregularity has a transition thickness as large as 100 meters (which is about a wavelength in a typical experiment), then equation (10) is a poor approximation. However, the correction factor will be a function only of wavelength, and since both modes have about the same wavelength, equation (11) can still be used. This point is discussed further in references 1, 3, and 5, and it is examined critically later in this report.

Equation (11), of course, specifies the phase difference, as well as the amplitude ratio of the reflected waves. Since they both depend on the same assumptions, one is about as well known as the other in a given experimental situation.

Effect of the Medium on Amplitude Ratio and Phase Difference

In order to have a useful diagnostic technique, both the phase difference produced by propagation in the medium under test and its derivative with respect to height must be large enough to measure. The phase difference for electron density and collision frequency profiles taken from reference 4 was calculated for this report. These profiles are shown in figure 1. The frequency, magnetic field, and propagation angle used in

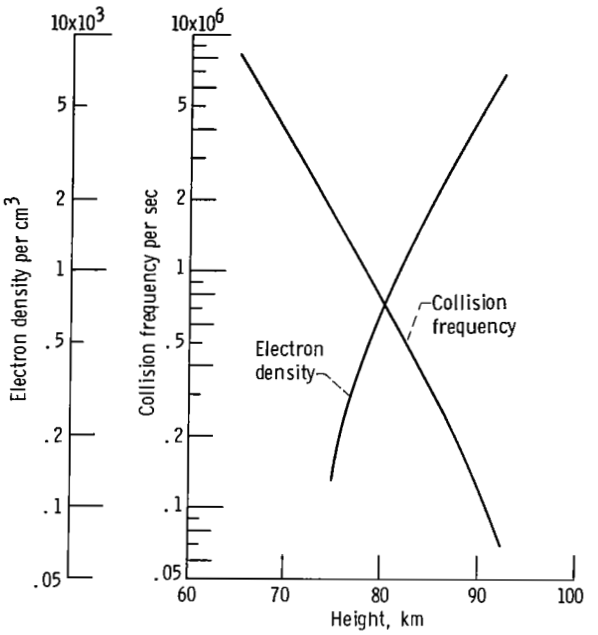

Figure 1. - Electron density and collision frequency as functions of height. (From ref. 4.)

these calculations are identical to those quoted for the experiment which produced the electron density profile (2.54 MHz, 4.3×10^{-5} T, and 40^{o}). Complex indexes of refraction were calculated by using the full theory of Sen and Wyller (ref. 14). The semiconductor integrals in the Sen-Wyller theory were computed by using the approximations of Burke and Hara (ref. 15).

Figure 2 shows the differential phase information calculated from this data. It is clear that the phase difference as measured on the ground (curve c) is comfortably large and rapidly varying throughout the height range shown. In addition, curves a and c almost coincide above about 80 kilometers. The phase difference imposed by the reflection process (phase of R_e/R_o) could almost be ignored in this height range. A phase-angle measurement which was accurate within a few degrees would produce an acceptable measurement of $\mathrm{Re}(n_o - n_e)$ throughout this height range. With increasing height, the measurement would become progressively more accurate, and the correction due to phase change on reflection would become progressively less important.

Another feature of the differential phase method is shown in figure 3. Values of $\mu = \mathrm{Re}(n_o - n_e)$ and $K = \mathrm{Im}(n_o - n_e)$ are plotted for three different collision-frequency profiles. In each case, the electron density profile used was the one shown in figure 1. The collision frequency profile in figure 1 was used to calculate the curves marked μa and Ka in figure 3. For the μb and Kb curves, the collision-frequency profile was multiplied by 0.5, and for the μc and Kc curves it was multiplied by 1.5.

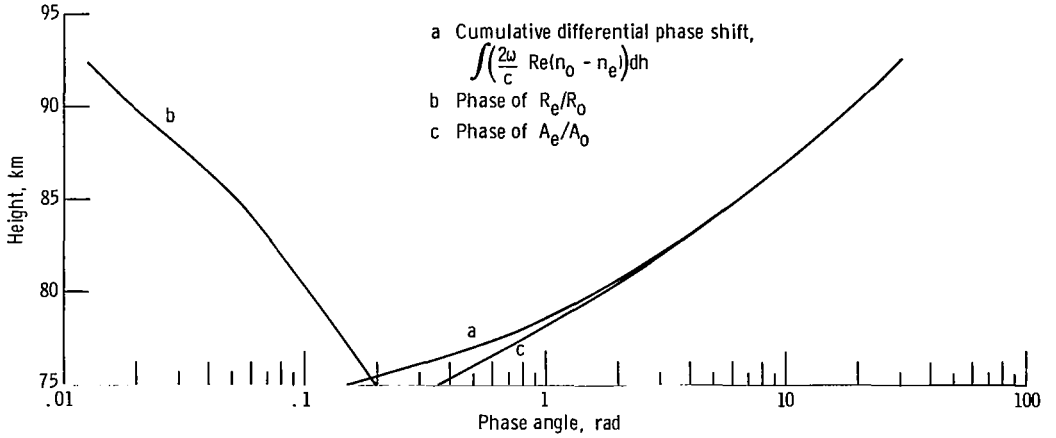

Figure 2. - Differential phase information as a function of height.

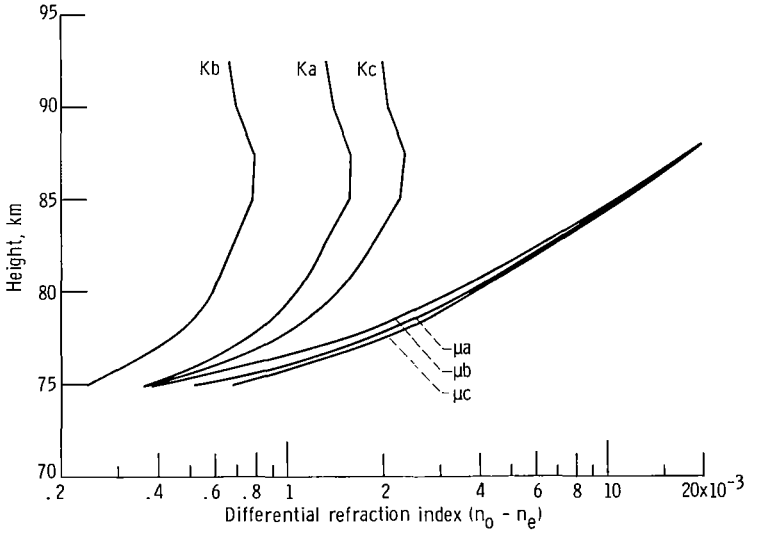

Figure 3. - Differential refractive index as a function of height.

Despite the wide variation in assumed collision profiles, the three curves for μ differed only slightly above 80 kilometers. The three curves for K differed markedly throughout the height range in question. It is easily shown through the Appleton-Hartree theory that μ is proportional to X alone and K is proportional to XZ when both X and Z are small. Figures 2 and 3 together illustrate a great potential advantage for the differential phase method above 75 or 80 kilometers. The differential absorption method requires an accurate predetermination of collision frequency. This is necessary to calculate the ratio $|R_e/R_o|$ and also to calculate a profile of N_e from a profile of $\mathrm{Im}(n_o - n_e)$. Figures 2 and 3 indicate that the differential phase method can get by with a rough estimate of collision frequency.

Although these remarks do not apply below 75 kilometers, there is still an important role for the differential phase experiments. Differential phase measurements could be used to accurately measure the electron density for heights greater than 75 or 80 kilometers. A differential absorption measurement could then be used to improve the estimate of collision frequency. The improved collision-frequency profile could then be extended downwards by using the known dependence of collision frequency on pressure (ref. 16).

In addition, the differential phase measurement should be useful to a somewhat higher altitude than the differential absorption measurement in a given experiment. The accuracy of differential absorption experiments often deteriorates above 85 kilometers because the weak extraordinary mode echo from this level is contaminated by oblique echoes from lower levels. The resultant errors in the extraordinary mode amplitude and phase, of course, cause errors in the amplitude and phase of A_o/A_e.

The sensitivity of the differential absorption experiment to these errors can be inferred from figure 4. In the experiments described in reference 4, the electron density was determined from the amount of change in amplitude ratio in each 2.5-kilometer height interval. Curve c of figure 4 shows that the amplitude ratio changed by about

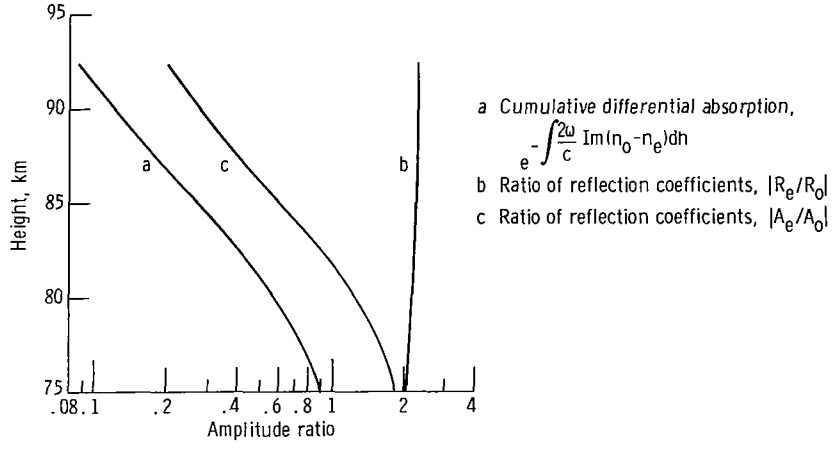

Figure 4. - Differential amplitude as function of height.

30 percent in a 2.5-kilometer height interval near 90 kilometers. Thus, a spurious signal that caused an amplitude error of the order of 30 percent could destroy the desired information.

A spurious signal of the same amplitude would cause a phase error of the order of 30 percent of a radian. But figure 2 shows that the differential phase shift changes by about 10 radians in the same 2.5-kilometer height interval. The differential phase shift is such a large effect in this height range that spurious signals would not cause appreciable errors until their amplitude exceeded that of the desired signal. Both methods

would then fail.

In the lower part of the D region, the addition of phase difference measurements will at least add a consistency check on some of the assumptions made in the experiment. In addition, as pointed out in reference 8, they may shed some light on the nature of the irregularities. There are, therefore, a number of compelling reasons for expending the effort necessary to add phase difference measurements to differential absorption experiments on a routine basis.

VERTICAL SCALE OF REFLECTING LAYERS

It is generally assumed that the ratio of reflection coefficients does not depend on the vertical scale of the reflecting layer (refs. 5 and 12). The justification is quite reasonable and goes somewhat as follows: For each mode, the reflection coefficient will be given by the Fresnel reflection coefficient multiplied by some geometrical factor $F(n, L)$. Here, L is the thickness of the layer in units of $2\pi c/\omega$, and n is the index of refraction. For both modes, the geometrical factors are generated by the same function, since the differential equations (the wave equations) for both modes are the same. The ratio of reflection coefficients, as given by equation (11), is in error by the factor

$$D(n_o, n_e, L) = \frac{F(n_o, L)}{F(n_e, L)} \tag{12}$$

which approximately equals unity, since $n_o \approx n_e$. The argument fails only if $F(n, L)$ is a rapidly varying function of n. It will be shown that $D(n_o, n_e, L)$ may sometimes differ appreciably from unity on this account.

The argument is presented in appendix B that the most reasonable way to represent a transition in electron density is with an Epstein profile. A suitable profile for generalizing a step change to one over a nonzero distance is

$$n^2(z) = n_1^2 + \frac{\left(n_2^2 - n_1^2\right)e^u}{e^u + 1} \tag{13}$$

where $u = z/\sigma$, and n_1 and n_2 are the indices of refraction below and above the transition. This profile is discussed in appendix B, and its reflection coefficient is given by equation (B3), which is repeated here for convenience

$$R = \frac{n_1 - n_2}{n_1 + n_2} \frac{(-2i\sigma k n_1)!}{(2i\sigma k n_1)!} \left\{ \frac{[i\sigma k(n_1 + n_2)]!}{[i\sigma k(n_1 - n_2)]!} \right\}^2 \tag{14}$$

If n_1 and n_2 are real, it can be shown that

$$R^2 = \frac{\sinh^2[\pi\sigma k(n_1 - n_2)]}{\sinh^2[\pi\sigma k(n_1 + n_2)]} \tag{15}$$

We are interested in cases where n_1 and n_2 are quite close to unity. The range of interest of σk is from zero to about 2π. Since the change in electron density is assumed to be small compared to the average value, n_1 and n_2 can be replaced by n, unless they occur in the combination $n_1 - n_2$. A reasonable approximation to equation (15) is then

$$R \approx \pm \frac{\pi\sigma k(\Delta n)}{\sinh(2\pi\sigma k n)} \tag{16}$$

where $\Delta n = n_1 - n_2$. The ratio of ordinary mode to extraordinary mode reflection coefficients is

$$\frac{R_o}{R_e} \cong \frac{\Delta n_o}{\Delta n_e} \frac{\sinh(2\pi\sigma k n_e)}{\sinh(2\pi\sigma k n_o)} \tag{17}$$

Since the right side of equation (16) is assumed real, R is specified with only a sign ambiguity. The sign will be the same for both modes, so there is no sign ambiguity in equation (17). The correction factor D is then given by

$$D(n_o, n_e, \sigma) \cong \frac{\sinh(2\pi\sigma k n_e)}{\sinh(2\pi\sigma k n_o)} \tag{18}$$

If L is defined in a reasonable way (appendix B),

$$\sigma = 0.228\ L \tag{19}$$

Equations (15) to (18) are deficient in two related respects. They depend on the assumption that n_1 and n_2 are real. They also contain no phase information. To improve on this, an approximate relation is obtained directly from equation (14). The indexes of refraction n_1 and n_2 are replaced by n, except where they occur as a factor $(n_1 - n_2)$. The factorial function $[i\sigma k(n_1 - n_2)]!$ can be replaced by unity as long as $|\sigma k(n_1 - n_2)|$ is small compared with unity.

$$R \cong \frac{n_1 - n_2}{2n} (-2i\sigma kn)!\,(2i\sigma kn)! \tag{20}$$

$$R \cong + \frac{\Delta n}{2} \frac{2\pi i\sigma k}{\sin(2\pi i\sigma kn)} \tag{21}$$

$$R \cong \frac{\pi\sigma k\,\Delta n}{\sinh(2\pi\sigma k\mu)\cos(2\pi\sigma kK) + i\cosh(2\pi\sigma k\mu)\sin(2\pi\sigma kK)} \tag{22}$$

where μ and K are the real and imaginary parts of n.

$$n_{o,\,e} = \mu_{o,\,e} + iK_{o,\,e} \tag{23}$$

It then follows that

$$D(n_o, n_e, \sigma) = \frac{\sinh(2\pi\sigma k\mu_e)\cos(2\pi\sigma kK_e) + i\cosh(2\pi\sigma k\mu_e)\sin(2\pi\sigma kK_e)}{\sinh(2\pi\sigma k\mu_o)\cos(2\pi\sigma kK_o) + i\cosh(2\pi\sigma k\mu_o)\sin(2\pi\sigma kK_o)} \tag{24}$$

Equations (22) and (24), of course, degenerate into equations (16) and (18) if K_o and K_e are set equal to zero.

To estimate the size of this effect, R_o, R_e, and $D(n_o, n_e, \sigma)$ are calculated by using equations (22) and (24) and the quasi-longitudinal approximation to the Appleton-Hartree equations. The calculations were made for experimental data taken from references 3 and 4. The data of reference 4 are shown in figure 1, and the data of reference 3 are shown in figure 5. Calculations were made for 1-, 5-, and 25-percent increases in electron density. The characteristic length σ was varied from 10 to 50 meters in steps of 10 meters. These ranges are consistent with parameters attributed to the irregularities by other authors (refs. 12 and 13).

There was an additional constraint placed on the irregularities considered. An irregularity was considered realistic if it produced a reasonable reflection coefficient. The range of reflection coefficients observed by experimenters varied from 10^{-3}

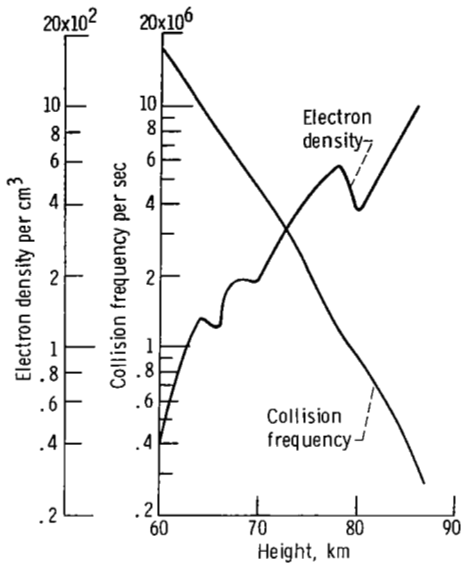

Figure 5. - Electron density and collision frequency as functions of height. (From ref. 3.)

(ref. 12) to 10^{-6} (ref. 13). We accordingly limit consideration to irregularities such that the larger of R_o and R_e falls in this range. Under this criterion, irregularities with a transition length σ greater than 40 meters never produced a large enough reflection coefficient. And 40 meters qualified in only one or two cases.

The magnitude of the geometrical factor $D(n_o, n_e, \sigma)$ is plotted against height for a number of irregularities in figures 6 and 7. Figure 6 contains the results of calculations using the data of reference 3, and figure 7 contains the results obtained with the data of reference 4. Figure 6 shows that the maximum probable error in the amplitude ratio due to this effect was somewhere between 5 and 10 percent in the experiments of reference 3. The experiments of reference 4 were performed up to much higher electron densities and were hence more susceptible to this particular error. Figure 7 shows that the expected errors in their amplitude ratios range up to about 30 percent.

In both of the above referenced experiments, other errors were present as large as those we are discussing. These other errors were due to such things as oblique reflections and inadequate isolation between channels. They could presumably be reduced by better experimental apparatus. The errors discussed here are more fundamental in nature and stem from inadequate knowledge of the geometry of the reflection-producing irregularities. This geometry varies randomly in both time and space. We believe this limits the potential accuracy of the differential absorption measurements to about their present capability.

In both cases discussed above, the phase of $D(n_o, n_e, \sigma)$ was calculated, as well as the amplitude. A plot was considered unnecessary, however, since for cases of inter-

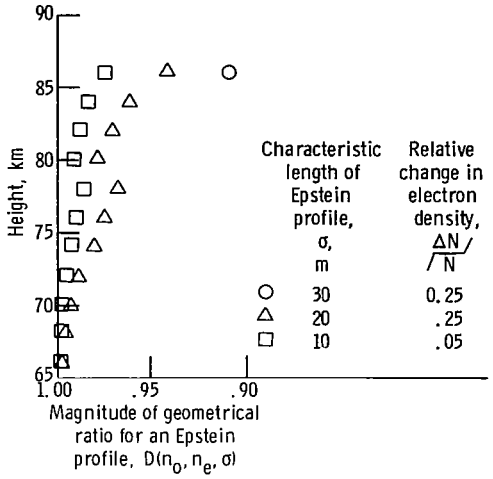

Figure 6. - Magnitude of geometrical ratio for an Epstein profile $D(n_o, n_e, \sigma)$ as a function of height for data of figure 5. Frequency, 2.66 megahertz; parameter Y_L, 0.58; parameter Y_T, 0.16.

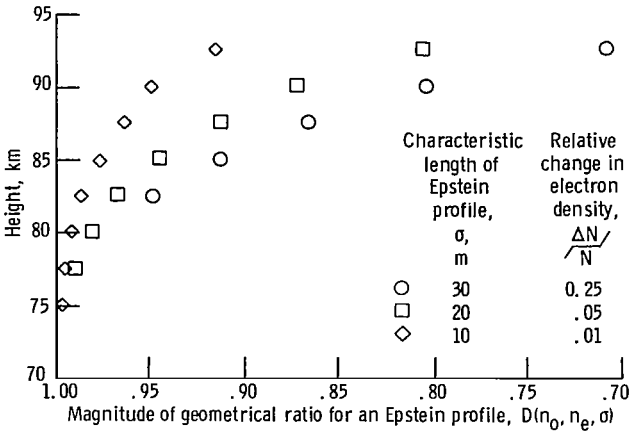

Figure 7. - Magnitude of geometrical ratio for an Epstein profile $D(n_o, n_e, \sigma)$ as a function of height for data of figure 1. Frequency, 2.54 megahertz; parameter Y_L, 0.36; parameter Y_T, 0.31.

est, the phase angle never exceeded 1^o. Apparently, then, this type of uncertainty about the reflecting layer will not be a factor in differential phase measurements. This latter result probably justifies discarding equation (24) in favor of the simpler equation (18) in qualitative discussions of this effect. In fact, equation (18) can be simplified even further. Unless σ is very small (less than approximately $\lambda/4\pi^2$), equation (18) is adequately approximated by

$$D(n_o, n_e, \sigma) \cong e^{2\pi\sigma k(\mu_e - \mu_o)} \tag{25}$$

Equation (25) can be used to estimate an effect of increased operating frequency. The collision-free quasi-longitudinal approximation to the Appleton-Hartree equations will suffice for μ_o and μ_e.

$$\mu_{o,e} \approx 1 - \frac{X}{2(1 \pm Y_L)} \tag{26}$$

and

$$\mu_o - \mu_e \approx \frac{XY_L}{1 - Y_L^2} \tag{27}$$

which behaves approximately as ω^{-3}. Thus, the exponent $2\pi\sigma k(\mu_e - \mu_o)$ behaves approximately as ω^{-2} for a given irregularity and would rapidly approach zero with increasing ω.

Increased operating frequency, of course, is desirable for other reasons. One of the most important sources of error in partial reflection experiments is oblique echoes. For a given antenna size, increased operating frequency allows a more collimated beam. Increased operating frequency, however, results in much weaker echoes. The reason is easily seen from equation (16). If σ is not too small ($\sigma \gtrsim \lambda/4\pi^2$), equation (16) can be approximated by

$$|R| \sim 2\pi\sigma k \, \Delta n e^{-2\pi\sigma k n} \tag{28}$$

which behaves approximately as $\omega^{-1} e^{-2\pi\sigma\omega/c}$. Thus, $|R|$ decreases exponentially with increasing ω. We expect, however, that a substantial decrease in echo strength can be tolerated. Thompson scatter measurements are routinely performed using echoes that are many orders of magnitude weaker than present partial reflection returns. The Thompson scatter echo return strength from the E region is equivalent to a voltage reflection coefficient of about 10^{-11}. The major cost is in time resolution, since it is necessary to integrate the signal over many pulses. The same techniques should be adaptable to partial reflection measurements.

MODE COUPLING ON REFLECTION

In some partial reflection experiments, only one magnetoionic mode is transmitted at a time. The ordinary and extraordinary waves are transmitted on alternate pulses (ref. 8). In other experiments, both modes are transmitted simultaneously, in the form of a linearly polarized wave (ref. 5). The reflected energy is separated into ordinary and extraordinary mode components by the receiving equipment used.

In simultaneous measurements, experimenters take great pains to minimize coupling between channels, since this is a potential source of error, particularly when one signal is much stronger than the other. The coupling between modes that may occur in the reflection process is usually not discussed.

If the irregularities are treated as plane discontinuities, the problem can be formulated simply by matching electric and magnetic fields across the interface (see appendix C and ref. 17). The resulting matrix equation can be solved numerically (ref. 17) or by the perturbation technique developed in appendix C.

We prefer, however, to avoid assuming that the irregularities are plane discontinuities. It is more likely that the changes in electron density take place over a signifi-

cant fraction of a wavelength. An adequate theory is available in the first-order coupled equations first given by Clemmow and Heading (ref. 18) and discussed by Budden (ref. 11). In the case of vertical incidence, the four coupled equations are given in reference 11.

$$f_1' + in_o f_1 = -\frac{n_o'}{2in_o} f_2 + i\frac{\psi}{2}\frac{(n_o + n_e)}{\sqrt{n_o n_e}} f_3 + \frac{\psi}{2}\frac{(n_o - n_e)}{\sqrt{n_o n_e}} f_4 \tag{29}$$

$$f_2' - in_o f_2 = \frac{n_o'}{2in_o} f_1 + \frac{\psi}{2}\frac{(n_o - n_e)}{\sqrt{n_o n_e}} f_3 - \frac{i\psi}{2}\frac{(n_o + n_e)}{\sqrt{n_o n_e}} f_4 \tag{30}$$

$$f_3' + in_e f_3 = -\frac{i\psi}{2}\frac{(n_o + n_e)}{\sqrt{n_o n_e}} f_1 - \frac{\psi}{2}\frac{(n_o - n_e)}{\sqrt{n_o n_e}} f_2 + \frac{n_e'}{2in_e} f_4 \tag{31}$$

$$f_4' - in_e f_4 = -\frac{\psi}{2}\frac{(n_o - n_e)}{\sqrt{n_o n_e}} f_1 + \frac{i\psi}{2}\frac{(n_o + n_e)}{\sqrt{n_o n_e}} f_2 - \frac{n_e'}{2in_e} f_3 \tag{32}$$

In equations (29) to (32), ψ is a coupling parameter given by

$$\psi = \frac{p_o'}{p_o^2 - 1} = \frac{p_e'}{p_e^2 - 1} \tag{33}$$

The subscripts "o" and "e" refer to ordinary and extraordinary waves, respectively. A prime denotes (1/k)(d/dz) (the calculation is performed in a coordinate system with length unit $\lambda/2\pi$). Here k and λ denote the free space wave number and wavelength. The polarizations for the two modes are p_o and p_e. It can be shown from the form of equations (29) to (32) that f_1 and f_2 are potentials for the upgoing and downgoing ordinary waves. In addition, f_3 and f_4 are potentials for the upgoing and downgoing extraordinary waves. Note that all terms on the right sides of equations (29) to (32), the coupling terms, contain spatial derivatives and would vanish in a homogeneous medium.

The fields are related to the potentials by

$$E_x = -\left[2\left(p_o^2 - 1\right)\right]^{-1/2}\left(n_o^{-1/2} f_1 + in_o^{-1/2} f_2 + ip_o n_e^{-1/2} f_3 + p_o n_e^{-1/2} f_4\right) \tag{34}$$

$$E_y = -\left[2\left(p_o^2 - 1\right)\right]^{-1/2}\left(p_o n_o^{-1/2} f_1 + i p_o n_o^{-1/2} f_2 + i n_e^{-1/2} f_3 + n_e^{-1/2} f_4\right) \tag{35}$$

$$Z_o H_x = \left[2\left(p_o^2 - 1\right)\right]^{-1/2}\left(p_o n_o^{1/2} f_1 - i p_o n_o^{1/2} f_2 + i n_e^{1/2} f_3 - n_e^{1/2} f_4\right) \tag{36}$$

$$Z_o H_x = \left[2\left(p_o^2 - 1\right)\right]^{-1/2}\left(-n_o^{1/2} f_1 + i n_o^{1/2} f_2 - i p_o n_e^{1/2} f_3 + p_o n_e^{1/2} f_4\right) \tag{37}$$

where Z_o is the characteristic impedance of free space. Consider a situation where there is an ordinary wave incident from below. The upgoing ordinary electric field is then

$$\vec{E}_{io} = -\left[2\left(p_o^2 - 1\right)\right]^{-1/2} n_o^{-1/2} f_1\left(\vec{a}_x + p_o \vec{a}_y\right) \tag{38}$$

The reflected (i. e., downgoing ordinary) electric field is

$$\vec{E}_{ro} = -\left[2\left(p_o^2 - 1\right)\right]^{-1/2} i n_o^{-1/2} f_2\left(\vec{a}_x + p_o \vec{a}_y\right) \tag{39}$$

The downgoing extraordinary electric field is

$$\vec{E}_{re} = -\left[2\left(p_o^2 - 1\right)\right]^{-1/2} n_o^{-1/2}\left(p_o \vec{a}_x + \vec{a}_y\right) f_4 \tag{40}$$

$$= -\left[2\left(p_o^2 - 1\right)\right]^{-1/2} n_e^{-1/2} p_o f_4\left(\vec{a}_x + p_e \vec{a}_y\right) \tag{41}$$

If the reflection coefficients are defined in terms of the x component of electric field, they are given by

$$R_{oo} = \frac{E_{rox}}{E_{iox}} = \frac{i f_2}{f_1} \tag{42}$$

$$R_{oe} = \frac{E_{rex}}{E_{iox}} = \frac{n_e^{-1/2} p_o f_4}{n_o^{-1/2} f_1} \tag{43}$$

For our purposes, the irregularities can be considered as small perturbations in $n_{o,e}$ and $p_{o,e}$. We can, therefore, use a Born approximation approach to the solutions of equations (29) to (32). Let the zero-order upward-propagating ordinary wave be given by

$$f_1^{(0)} = e^{-in_o z} \tag{44}$$

and let all other zero-order waves be zero. Then the first-order equations for the downward-propagating ordinary and extraordinary waves are

$$f_2^{(1)'} - in_o f_2^{(1)} = \frac{n_o'}{2in_o} f_1^{(0)} = \frac{n_o'}{2in_o} e^{-in_o z} \tag{45}$$

and

$$f_4^{(1)'} - in_e f_4 = -\frac{1}{2}\psi \frac{(n_o - n_e)}{\sqrt{n_o n_e}} e^{-in_o z} \tag{46}$$

Equations (45) and (46) can be solved by elementary methods to yield the first-order equations

$$f_2^{(1)} = -e^{in_o z} \int_z^\infty \frac{n_o'}{2in_o} e^{-2in_o z_1} dz_1 \tag{47}$$

and

$$f_4^{(1)} = -e^{in_e z} \int_z^\infty -\frac{\psi}{2} \frac{(n_o - n_e)}{\sqrt{n_o n_e}} e^{-i(n_o+n_e)z_1} dz_1 \tag{48}$$

Since we are only interested in the first Born approximation, we will henceforth drop the superscript (1). We will set $z = 0$ at the lower edge of the irregularity and refer our reflection coefficients to this point. With these adjustments, equations (47) and (48) become

$$f_2 = -\int_0^\infty \frac{n_o'}{2in_o} e^{-2in_o z_1}\, dz_1 \tag{49}$$

and

$$f_4 = -\int_0^\infty -\frac{1}{2}\frac{(n_o - n_e)}{\sqrt{n_o n_e}}\frac{p_o'}{p_o^2 - 1} e^{-i(n_o+n_e)z_1}\, dz_1 \tag{50}$$

Equation (33) has been used to eliminate ψ. Now $n_{o,e}$ and $p_{o,e}$ contain the irregularity as a small perturbation. But $n'_{o,e}$ and $p'_{o,e}$ are first order in the irregularity. It is consistent with this first-order approximation to use the unperturbed (zero order) values for $n_{o,e}$ and $p_{o,e}$. Thus,

$$f_2 \cong \frac{-1}{2in_o}\int_0^\infty n_o' e^{-2in_o z}\, dz \tag{51}$$

and

$$f_4 \cong +\frac{1}{2}\frac{(n_o - n_e)}{\left(p_o^2 - 1\right)\sqrt{n_o n_e}}\int_0^\infty p_o' e^{-i(n_o+n_e)z}\, dz \tag{52}$$

Reflection From a Plane Discontinuity

The plane discontinuity is the limiting case of a transition that takes place in a distance small compared to a wavelength (say δ). The integrals are easily evaluated for this special case. Then,

$$\int_0^\infty n_o' e^{-2in_o z}\, dz \cong \int_0^\delta n_o'\, dz = \Delta n_o \tag{53}$$

Similarly,

$$\int_0^\infty p_o' \, e^{-i(n_o+n_e)z} \, dz \cong \Delta p_o \tag{54}$$

Thus,

$$f_2 \cong -\frac{\Delta n_o}{2in_o} \tag{55}$$

$$f_4 \cong \frac{1}{2} \frac{(n_o - n_e)\Delta p_o}{\left(p_o^2 - 1\right)\sqrt{n_o n_e}} \tag{56}$$

and

$$R_{oo} = -\frac{\Delta n_o}{2n_o} \tag{57}$$

$$R_{o,\,e} = \frac{1}{2} \frac{(n_o - n_e)\Delta p_o}{n_e(p_o - p_e)} \tag{58}$$

We have used equations (42) to (44) and the fact that $p_o p_e = 1$. Both results agree with the first-order results of appendix C.

Reflection From Finite Electron Density Irregularity

For this case,

$$n_o' = \frac{\partial n_o}{\partial X} X' \tag{59}$$

$$p_o' = \frac{\partial p_o}{\partial X} X' \tag{60}$$

where $\partial n_o/\partial X$ and $\partial p_o/\partial X$ are considered zero order. By using equations (51), (52), (59), and (60), we can write

$$f_2 \cong -\frac{1}{2in_o}\frac{\partial n_o}{\partial X}\int_0^\infty X' e^{-2in_o z}\,dz = -\frac{1}{2in_o} I_{oo}\frac{\partial n_o}{\partial X} \tag{61}$$

and

$$f_4 \cong \frac{(n_o - n_e)}{2\left(p_o^2 - 1\right)\sqrt{n_o n_e}}\frac{\partial p_o}{\partial X}\int_0^\infty X' e^{-i(n_o+n_e)z}\,dz = \frac{(n_o - n_e)}{2\left(p_o^2 - 1\right)\sqrt{n_o n_e}}\frac{\partial p_o}{\partial X} I_{oe} \tag{62}$$

The reflection coefficients defined in terms of the x component of electric field will be

$$R_{oo} \cong -\frac{1}{2n_o}\frac{\partial n_o}{\partial X} I_{oo} \tag{63}$$

and

$$R_{oe} \cong \frac{(n_o - n_e)}{2(p_o - p_e)n_e}\frac{\partial p_o}{\partial X} I_{oe} \tag{64}$$

We defined our reflection coefficients this way in appendix C to compare our results with those of reference 17. It is more reasonable, however, to present results in terms of the magnitude of the electric fields rather than their x component. Accordingly, we define $\mathscr{R}_{ab}$ as the magnitude of the electric field of the reflected b mode divided by the magnitude of the electric field of the incident a wave. This definition assumes that both fields are measured at the same point and that only one incident wave is present. It is easily shown that

$$\mathscr{R}_{oo} = |R_{oo}| \cong \left|\frac{1}{2n_o}\frac{\partial n_o}{\partial X} I_{oo}\right| \tag{65}$$

and

$$\mathscr{R}_{oe} = |p_e R_{oe}| \cong \left| \frac{(n_o - n_e)}{2\left(p_o^2 - 1\right) n_e} \frac{\partial p_o}{\partial X} I_{oe} \right| \tag{66}$$

A similar analysis can be performed by assuming an incident extraordinary wave. The results are

$$\mathscr{R}_{ee} \cong \left| \frac{1}{2n_e} \frac{\partial n_e}{\partial X} I_{ee} \right| \tag{67}$$

and

$$\mathscr{R}_{eo} \cong \left| \frac{(n_o - n_e)}{2\left(p_o^2 - 1\right) n_o} \frac{\partial p_o}{\partial X} I_{eo} \right| \tag{68}$$

The shape of the irregularity enters only through the integrals I_{oo}, etc. Since $n_o \approx n_e$, however, all of these integrals have about the same value. The ratio of any two reflection coefficients is therefore almost independent of irregularity thickness and form. This is analogous to assuming that the correction factor $D(n_o, n_e, \sigma)$ discussed earlier is equal to unity. We found errors up to 30 percent in this latter assumption. Such errors would be quite tolerable, however, in the present application where we merely attempt to determine whether errors due to cross reflection are likely to be appreciable in a given experiment. The two ratios of interest are

$$C_{eo} = \frac{\mathscr{R}_{eo}}{\mathscr{R}_{oo}} \approx \left| \frac{(n_o - n_e)}{\left(p_o^2 - 1\right)} \frac{\partial p_o / \partial X}{\partial n_o / \partial X} \right| \tag{69}$$

and

$$C_{oe} = \frac{\mathscr{R}_{oe}}{\mathscr{R}_{ee}} \cong \left| \frac{(n_o - n_e)}{\left(p_o^2 - 1\right)} \frac{\partial p_o / \partial X}{\partial n_e / \partial X} \right| \tag{70}$$

Equation (69) gives the ratio of reflected o wave electric fields produced by equal-amplitude incident e and o waves. It is thus a measure of the degree to which the reflected o wave is contaminated by energy coupled in from the incident e wave.

Equation (70) similarly gives a measure of reflected e wave contamination by coupling to the incident o wave. Since equations (69) and (70) do not depend on the shape of the reflecting layer, the magnitude of the coupling effect can be estimated without any knowledge of the layer.

Figures 8 to 10 show sample calculations performed by using equations (69) and (70). The wave frequency was taken as 2.5 megahertz and the collision frequency as 10^5 per second which is a reasonable value for the 90-kilometer altitude. Because of the factor $(n_o - n_e)$ in equations (69) and (70), the coupling ratios would be appreciable only in the upper part of the range of electron densities of interest. In our sample calculations, the range chosen was from 2000 to 10 000 per cubic centimeters.

Figure 9 shows both coupling ratios plotted as functions of propagation angle for an electron density of 10^4 per cubic centimeter and a magnetic field of 5×10^{-5} tesla (0.5 gauss). In figures 9 and 10, the ratios C_{oe} and C_{eo}, respectively, are plotted against electron density for three representative magnetic field orientations. The three cases are (1) magnetic field strength (B) of 0.35×10^{-4} tesla and propagation angle (φ) of 75^o; (2) magnetic field strength of 0.5×10^{-4} tesla and propagation angle of 45^o; and

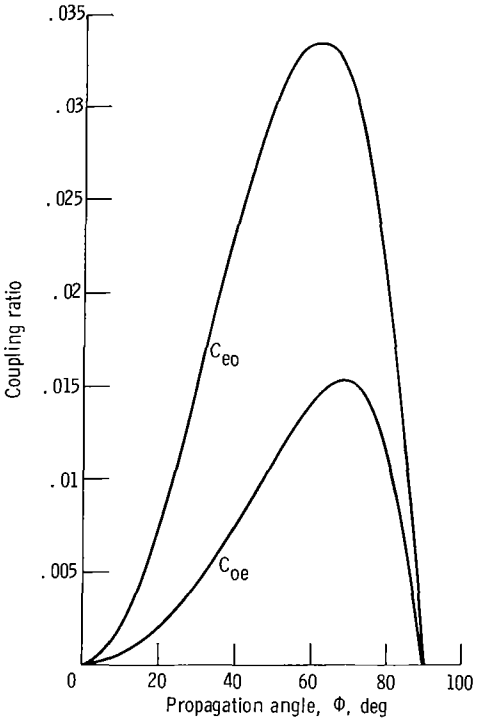

Figure 8. - Coupling ratio as a function of propagation angle. Wave frequency, 2.5 megahertz; magnetic field, 5×10^5 tesla; electron density, 10^4 per cubic centimeter; collision frequency, 10^5 per second.

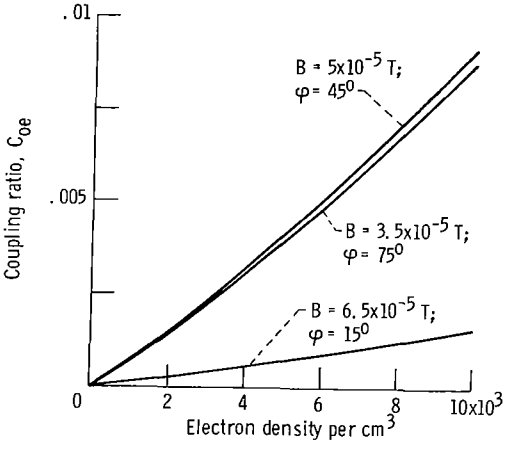

Figure 9. - Coupling ratio, C_{oe}, as a function of electron density. Wave frequency, 2.5 megahertz; collision frequency, 10^5 per second.

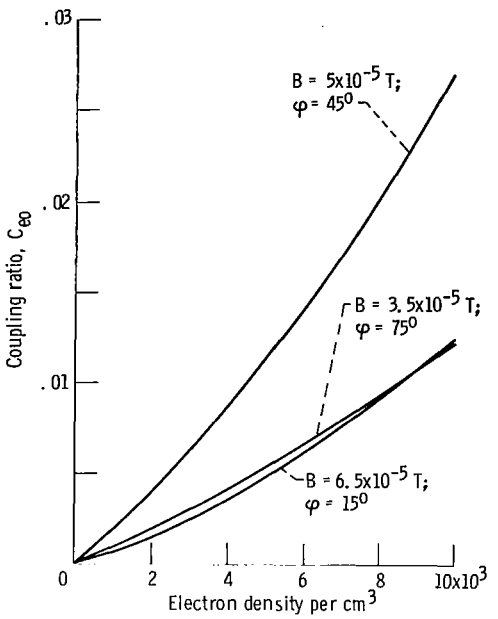

Figure 10. - Coupling ratio, C_{eo}, as a function of electron density. Wave frequency, 2.5 megahertz; collision frequency, 10^5 per second.

(3) magnetic field strength of 0.65×10^{-4} tesla and propagation angle of 15°. These are chosen to represent near-equatorial, mid, and near-polar latitude, respectively. The calculated coupling ratios range up to about 1 percent for C_{oe} and 3 percent for C_{eo}. It should be noted that, due to differential absorption, the incident ordinary wave could be an order of magnitude stronger than the incident extraordinary wave at the 90-kilometer level. The effect of o-e coupling would be greatly augmented by this disparity in incident wave amplitude. This difference in incident wave amplitude would, of course, reduce the influence of mode coupling on the reflected ordinary wave.

The coupling ratios C_{oe} and C_{eo} have been found to be in the 1 to 3 percent range at an electron density of 10^4 per cubic centimeter. Because there can be a large disparity in incident amplitude, the spurious part of the reflected e wave might approach about 10 percent. This is not large enough to be important at the present state of the art. Partial reflection experiments are usually not performed above electron densities of about 2000 per cubic centimeter, and when they are, the higher altitude part of the data is taken with reservations (ref. 17). However, appreciable improvement in current experimental capability would probably make mode-coupling errors large enough that they should be taken into account.

REMARKS ON THE EFFECTS OF TURBULENCE

Our analysis of the reflection process have been one dimensional under the assumption that the reflections are from horizontally stratified layers with transverse dimensions at least comparable to the central Fresnel zone. The radius r of the central Fresnel zone is approximately

$$r \approx \sqrt{h\lambda} \tag{71}$$

where h is the height of the irregularity, and λ is the wavelength of the radiation. In these experiments, r is typically about 2 kilometers. The vertical scale of the irregularities must be much less, however, to produce the measured reflection coefficients.

At the opposite extreme, so to speak, one could view the irregularities as a sea of homogeneous turbulence filling the entire region of interest. The reflections from such irregularities can be discussed by using the Born approximation solutions of the wave equation and the statistical approach given in reference 19. The strength of the reflections would depend on the power spectrum of the irregularities (i. e., the Fourier transform of the electron density spatial autocorrelation function). The reflection strength for backscatter would be proportional to the Fourier component at $2\vec{k}_i$, where $\vec{k}_i$ is the incident wave propagation vector. Belrose and Burke (ref. 3) showed that, on the simplest level, the differential absorption method would work just as well even if this latter description of the irregularities were more correct. Flood (refs. 20 and 21) calculated a correction to this description explicitly taking into account differential absorption within the scattering volume. Flood also argued in favor of the "volume scattering" description of the irregularities. In reference 10, von Biel, Flood, and Camnitz, also argued the case for the "volume scattering" description, claiming that their experimental data ruled out the alternative. Conclusions drawn from the data of reference 10, however, should be considered tentative, since the data were reduced by using a questionable assumption. As mentioned earlier the data reduction theory of reference 10 assumed the validity of the quasi-longitudinal approximation. The experiments, however, were performed at a place in Brazil where the magnetic dip angle is about 30°. At a 60° propagation angle, the quasi-longitudinal approximation is somewhat doubtful at 2. 4 megahertz, the frequency at which the experiments were performed.

Belrose (ref. 8) takes the view that the process of reflection is probably not uniquely quasi-stratified or turbulent but is a combination of the two. If the irregularities are due to turbulent mixing of the existing electron density gradient, such a view is easy to justify. Bolgiano (ref. 22) discussed turbulent processes that might produce highly anisotropic irregularities with the characteristic vertical dimension much smaller than the horizontal. The transition length could be as small as the Kolmogoroff inner scale of

turbulence. This would be about 10 meters at the 100-kilometer altitude and would decrease with decreasing altitude. The irregularities would have horizontal structure on length scales up to that of the energy containing eddies. This might be tens of kilometers. The quasi-stratified view of the irregularities then is probably a reasonable starting point. Even with this simplified view, we have shown that significant errors may arise through ignorance of the irregularities. Other significant problems would emerge in a study which incorporated the effects of turbulence in a realistic way.

One such problem is connected with the pulsed nature of the transmissions. An important assumption in the partial reflection experiments is that, at a given time, both modes are reflected from the same height or range of heights. This need not be exactly true, since the group velocities for the two modes are different. The ordinary wave pulse will always lead the extraordinary wave pulse by a small distance, the "nonoverlap distance," Δh. It is easily shown that Δh is given approximately by

$$\Delta h \cong \int_0^h \left(1 - \frac{\mu_{ge}}{\mu_{go}}\right) dz \tag{72}$$

where μ_g is the group refractive index (c divided by the group velocity)

$$\mu_{go,\,e} = \frac{c}{v_{go,\,e}} = \mathrm{Re}\,\frac{\partial}{\partial \omega}\,\omega n_{o,\,e} \tag{73}$$

Figure 11 shows Δh as a function of height as computed from equation (72) by using the ionosphere of figure 1 and a frequency of 2.54 megahertz. Since a pulse length in partial reflection experiments is usually of the order of 5 kilometers, Δh is small compared to a pulse length at any level.

Whether the nonoverlap is a problem seems to depend on the mean vertical spacing of the reflecting irregularities. If the mean spacing of reflectors is large compared to the nonoverlap distance, then most of the time the ordinary and extraordinary mode pulses will illuminate the same reflectors. In particular, if the mean spacing is of the order of a pulse length, then the nonoverlap distance must approach a pulse length before we encounter difficulties on this score. For the conditions considered in figure 11, this clearly does not happen at any altitude of interest.

In the case of homogeneous turbulence, one can show (ref. 19) that the scattering comes primarily from the spatial Fourier component of the turbulence whose length scale is one-half of a wavelength. For this case, therefore, it is conceivable that our results might be modified when the nonoverlap distance is as small as one-half wavelength. For the conditions of figure 11, this occurs at a height of about 85 kilometers.

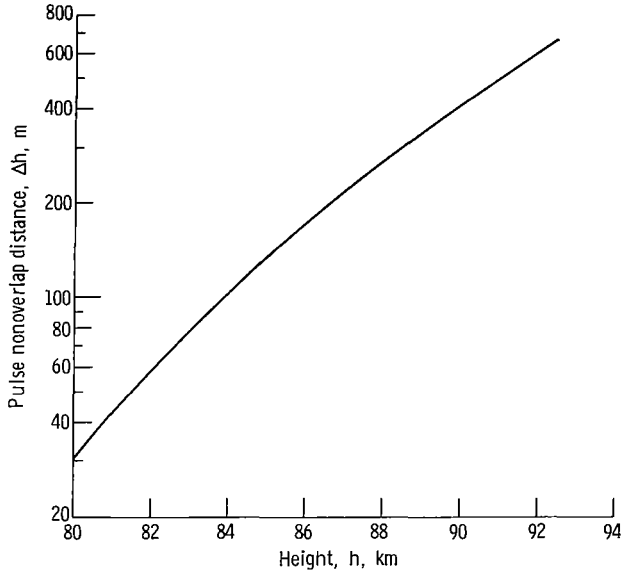

Figure 11. - Pulse nonoverlap distance as a function of height for a frequency of 2.54 megahertz and the ionosphere of figure 1.

This is, however, a very conservative estimate of when the nonoverlap is a problem, and further work should be done to analyze partial reflections from a turbulent region.

CONCLUDING REMARKS

We have discussed the addition of phase difference measurements to partial reflection experiments and some advantages in this method of measuring electron density were pointed out. In particular, the determination of electron density through phase difference measurements is much less sensitive to errors in the assumed collision frequency profile. Moreover, both electron density and collision frequency can be determined through measurements of differential absorption and phase shift.

In partial reflection experiments, the reflections are usually treated as simple Fresnel reflections from a plane interface. We have argued that the most reasonable one-dimensional model for the irregularities is an Epstein profile. We have shown that the ratio of reflection coefficients, as calculated for this type of profile, sometimes differs appreciably from the result given by Fresnel reflection. At a given operating frequency, errors due to this effect would increase with height (or electron density). The errors would, however, diminish rapidly with increased operating frequency.

We have also studied the effect of mode coupling in the reflection process. Calculations were made for a plane discontinuity and for a general one-dimensional model of

the reflecting layer. In both cases, mode coupling was found to be a fairly small effect. Its importance also increased with electron density, however, and our calculations indicate appreciable potential errors due to this effect in partial reflection measurements where the electron density is greater than or equal to 10^4 per cubic centimeter. It is easily shown that this effect also diminishes with increased operating frequency. In addition, the effect of mode coupling can be avoided by transmitting the two modes on alternate pulses.

The prevalent ideas on the nature of the reflecting irregularities were also discussed in the context of modern ideas on atmospheric turbulence. The quasi-stratified view of the irregularities was shown to be consistent with these ideas. The effect of differential group delay on partial reflection experiments was considered. It was found to be small compared to pulse width in a typical experimental situation. It is not considered an important source of error if the reflections are from a few discrete irregularities.

Lewis Research Center,
National Aeronautics and Space Administration,
Cleveland, Ohio, January 17, 1972,
112-02.

APPENDIX A

SYMBOLS

A_e	extraordinary wave reflection coefficient referred to ground
A_o	ordinary wave reflection coefficient referred to ground
a	constant in eq. (B7)
$\vec{a}_x$	unit vector in x direction
$\vec{a}_y$	unit vector in y direction
c	velocity of light in free space (3×10^8 m/sec)
c_1, c_2, c_3	constants in eq. (B1)
$D(n_o, n_e, L)$	geometrical ratio defined by eq. (12)
$D(n_o, n_e, \sigma)$	geometrical ratio for Epstein profile
d	length of linear transition (fig. 12)
E_x	electric field (x component)
E_y	electric field (y component)
E_{iox}	x component of $\vec{E}_{io}$
E_{rex}	x component of $\vec{E}_{re}$
E_{rox}	x component of $\vec{E}_{ro}$
$\vec{E}_{io}$	incident ordinary electric field
$\vec{E}_{re}$	reflected extraordinary electric field
$\vec{E}_{ro}$	reflected ordinary electric field
$F(n_e, L)$	geometrical factor in extraordinary wave reflection coefficient
$F(n_o, L)$	geometrical factor in ordinary wave reflection coefficient
f_1	potential for upgoing ordinary wave
f_2	potential for downgoing ordinary wave
f_3	potential for upgoing extraordinary
f_4	potential for downgoing extraordinary
h	height of reflection
I_{oe}	integral defined by eq. (62)

I_{oo} integral defined by eq. (61)

K imaginary part of $(n_o - n_e)$

K_e imaginary part of n_e

K_o imaginary part of n_o

k free space wave number

$\vec{k}_i$ incident wave propagation vector

L characteristic length (fig. 12)

$[M]$ coefficient matrix defined by eqs. (C9) and (C10)

m exponent in eq. (B7)

N electron density per cubic centimeter

n complex index of refraction

n_1 index of refraction below transition

n_2 index of refraction above transition

$n_a^{(1)}$ index of refraction of "a" wave in lower region

$n_a^{(2)}$ index of refraction of "a" wave in upper region

$n_b^{(1)}$ index of refraction of "b" wave in lower region

$n_b^{(2)}$ index of refraction of "b" wave in upper region

n_e index of refraction of extraordinary wave

n_o index of refraction of ordinary wave

$[P]$ column vector defined by eqs. (C9) and (C10)

$p_a^{(1)}$ polarization (E_y/E_x) of "a" wave in lower region

$p_a^{(2)}$ polarization of "a" wave in upper region

$p_b^{(1)}$ polarization of "b" wave in lower region

$p_b^{(2)}$ polarization of "b" wave in upper region

p_e extraordinary wave polarization

p_o ordinary wave polarization

q parameter defined by eq. (B9)

R reflection coefficient

$[R]$	column vector defined by eqs. (C9) and (C10)
r	radius of central Fresnel zone
R_{aa}	direct reflection coefficient for E_x
R_{ab}	cross reflection coefficient for E_x incident "a" wave, reflected "b" wave
R_e	extraordinary wave reflection coefficient referred to height of reflection
R_o	ordinary wave reflection coefficient referred to height of reflection
R_{oo}	ordinary wave direct reflection
R_{oe}	cross reflection coefficient, incident "o" wave, reflected "e" wave
T_{aa}	transmission coefficient for "a" wave
T_{ab}	cross transmission coefficient, incident "a" wave, transmitted "b" wave
T_D	wave transit time defined by eq. (B22)
u	normalized Cartesian coordinate (Z/σ)
W	parameter defined by eq. (B8)
W_0	W for $Z = 0$
W_e	parameter defined for extraordinary wave by eqs. (6) and (7)
W_o	parameter defined for ordinary wave by eqs. (6) and (7)
X	parameter proportional to electron density $\left(\omega_p^2/\omega^2\right)$
x	Cartesian coordinate
Y	normalized gyrofrequency (ω_b/ω)
Y_L	$Y \cos \varphi$
Y_T	$Y \sin \varphi$
y	Cartesian coordinate
Z	normalized collision frequency (ν/ω)
z	Cartesian coordinate
ϵ	electric permittivity
ϵ_0	electric permittivity of free space
λ	free space wave length
μ	real part of $(n_o - n_e)$
μ_0	magnetic permeability of free space
μ_e	real part of n_e

μ_o real part of n_o

ν electron collision frequency

ρ parameter defined by eq. (B10)

ρ_d parameter defined by eq. (B19)

ρ_0 parameter defined by eq. (B18)

σ characteristic length of Epstein profile

τ pulse length, sec

φ propagation angle relative to magnetic field

ψ coupling parameter defined by eq. (33)

ω angular frequency

ω_b electron gyrofrequency

ω_p plasma frequency

APPENDIX B

THE REFLECTION OF ELECTROMAGNETIC WAVES FROM A GRADIENT OF REFRACTIVE INDEX

The reflection coefficient of a transition between two different regions of constant refractive index has long been of interest (ref. 23). Solutions can be obtained for many different transition shapes. These transition shapes may be grouped into two general classes. One class comprises the smooth profiles. For this class, the index of refraction in the region of interest is specified by a single analytic function which is asymptotic to the desired constant end values. This class includes, but is not limited to, the so-called Epstein profiles (refs. 11 and 24).

The other class of transitions comprises the discontinuous profiles. They include all those that have a well-defined beginning and end. The index of refraction is described by specified constants outside the transition region. Inside the transition region, it is described by some function which is matched to the constant regions at the boundaries. The first derivative, however, or some higher order derivative is discontinuous at the boundaries. In this appendix, the solutions for both types of profiles are discussed, and it is shown that there are important differences. The reflection coefficients for discontinuous profiles have an oscillatory behavior as a function of wavelength. This is not present in the results for Epstein profiles. The reflection coefficients for discontinuous profiles are also very much larger in the short wavelength limit. We argue that the smooth profiles are most reasonable descriptions of a transition in electron density.

Epstein Profiles

A family of curves able to simulate a wide variety of electron density contours are the Epstein profiles (refs. 11 and 24). They are described by the relation (ref. 11)

$$n^2(z) = c_1 + \frac{e^u}{\left(e^u + 1\right)^2}\left[(c_2 - c_1)(e^u + 1) + c_3\right] \tag{B1}$$

where n is the index of refraction. Also,

$$u = \frac{z}{\sigma} \tag{B2}$$

where σ is a characteristic length. For these profiles, the wave equation can be transformed into the hypergeometric equation and exact solutions can be obtained.

We are interested in a continuous monotonic transition from index of refraction n_1 to index of refraction n_2. This is simulated by using $c_1 = n_1^2$, $c_2 = n_2^2$, and $c_3 = 0$. An

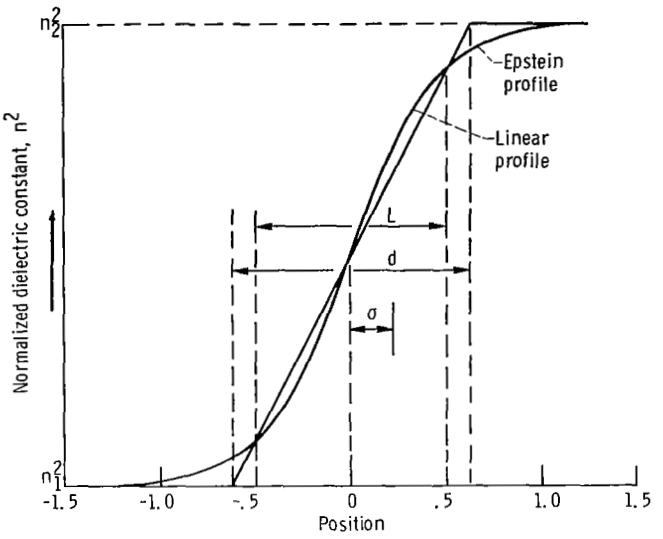

Figure 12. - Normalized dielectric constant as a function of position for linear profile and Epstein profile with parameters $c_1 = n_1^2$, $c_2 = n_2^2$, and $c_3 = 0$. Length L is distance for $(n_2^2 - n_1^2)$ to change from 10 percent to 90 percent of its final value; length of linear profile d is equal to 1.25L; characteristic length of Epstein profile σ is equal to 0.228L.

Epstein profile of this type is shown in figure 12. The electric field reflection coefficient for this case is given in reference 11 as

$$R = \frac{n_1 - n_2}{n_1 + n_2} \frac{(-2i\sigma k n_1)!}{(2i\sigma k n_1)!} \left\{ \frac{\left[i\sigma k(n_1 + n_2)\right]!}{\left[i\sigma k(n_1 - n_2)\right]!} \right\}^2 \tag{B3}$$

where $k = \omega/c$ is the free space wave number. If n_1 and n_2 are real, the magnitude of R may be expressed in a fairly simple form

$$|R|^2 = \left\{ \frac{\sinh\left[\pi\sigma k(n_1 - n_2)\right]}{\sinh\left[\pi\sigma k(n_1 + n_2)\right]} \right\}^2 \tag{B4}$$

In obtaining equation (B4), the following relation was used:

$$x!(-x)! = \frac{\pi x}{\sin \pi x} \tag{B5}$$

If the transition is very abrupt ($\sigma k \ll 1$), then equation (B4) reduces to the simple Fresnel reflection formula

$$R^2 = \left(\frac{n_1 - n_2}{n_1 + n_2}\right)^2 \tag{B6}$$

However, the reflection coefficient in equation (B4) drops off monotonically and very rapidly as σk is increased.

Discontinuous Profiles

A number of earlier investigators have calculated reflection coefficients for profiles with discontinuities in the gradient of dielectric constant. In many cases, these profiles are considered as approximations to a plasma boundary, that is, the lower edge of the ionosphere or a shock front (refs. 25 to 27). The discontinuity in gradient is usually considered as an unphysical but minor feature of the profile; one that should not appreciably effect the result.

Other authors have noticed that, in cases where the transition region is long compared to a wavelength, the discontinuity has a profound effect on the result. Schelkunoff (ref. 28) showed that the reflection coefficients of finite transitions are strongly dependent on the behavior of the impedance function at the boundaries. If the impedance function I and its first m derivatives are continuous at the boundaries of the layer but the (m + 1) derivative is not, then for a sufficiently small wavelength, the reflection coefficient varies as $(\lambda/d)^{m+1}$, where λ is the normal wavelength and d is the length of the transition region. This is true regardless of the precise functional form of I. Schelkunoff (ref. 28) also pointed out that Epstein profiles have a fundamentally different behavior in this range and warned against applying them to practical problems. Schelkunoff asserted that the difference was due primarily to the effect, on the reflected wave, of the semi-infinite regions, where the Epstein profile only approximates a constant. While this may be true, Schelkunoff's point of view ignores an even more unrealistic feature of the discontinuous profiles.

To illustrate this point, we consider a very old problem (ref. 23). We alter the ap-

proach slightly to obtain results in a form which best illustrates our point. Consider a transition in refractive index of the form

$$n^2 = \begin{cases} n_1^2 & \text{for } z < 0 \\ n_1^2(1 + az)^m & \text{for } 0 < z < d \\ n_1^2(1 + ad)^m = n_2^2 & \text{for } z > d \end{cases} \tag{B7}$$

A family of these profiles is shown in figure 13. The function $(1 + az)^m$ is plotted against z for various values of m. In each case, the constant a is chosen to bring

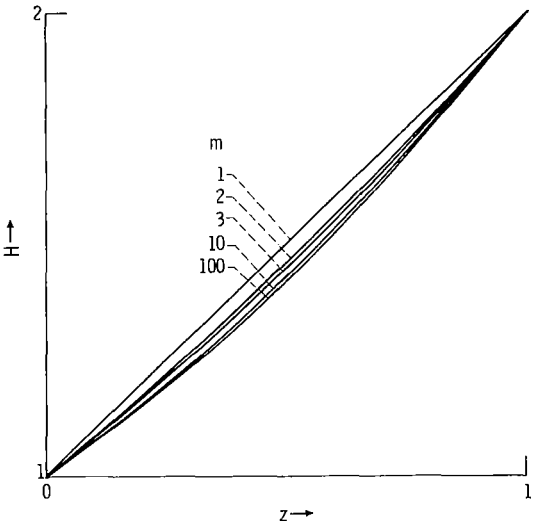

Figure 13. - Function $H = (1 + az)^m$ for various values of m. In each case, a is chosen to take the curve through the same end points.

the curve through the same end points. The shape of the curve is surprisingly insensitive to the value of the exponent m. These profiles are continuous at $z = 0$ and $z = d$, but the first derivative is not. We assume normal incidence and time dependence $e^{i\omega t}$. We also make the following definitions (still more or less following ref. 23):

$$W - W_0 = \int_0^z \sqrt{\epsilon_0 n}\, dz \tag{B8}$$

$$q = \frac{m + 1}{m + 2} \tag{B9}$$

$$\rho = \omega \sqrt{\mu_0}\, W \tag{B10}$$

By using these definitions, the wave equation in the transition region can be transformed to Bessel's equation. The solutions are matched to a transmitted wave on the right side and an incident plus reflected wave on the left side. The result for the reflection coefficient is

$$R = \frac{P_1 Q_2 - P_2 Q_1}{P_2 Q_3 - P_1 Q_4} \tag{B11}$$

where

$$Q_1 = H_q^{(1)}(\rho_0) - iH_{q-1}^{(1)}(\rho_0) \tag{B12}$$

$$Q_2 = H_q^{(2)}(\rho_0) - iH_{q-1}^{(2)}(\rho_0) \tag{B13}$$

$$Q_3 = H_q^{(1)}(\rho_0) + iH_{q-1}^{(1)}(\rho_0) \tag{B14}$$

$$Q_4 = H_q^{(2)}(\rho_0) + iH_{q-1}^{(2)}(\rho_0) \tag{B15}$$

$$P_1 = H_q^{(1)}(\rho_d) - iH_{q-1}^{(1)}(\rho_d) \tag{B16}$$

$$P_2 = H_q^{(2)}(\rho_d) - iH_{q-1}^{(2)}(\rho_d) \tag{B17}$$

$$\rho_0 = \rho(z = 0) \tag{B18}$$

$$\rho_d = \rho(z = d) \tag{B19}$$

If the transition region is long compared to a wavelength, then both ρ_0 and ρ_d are large compared to unity, and we can use asymptotic approximations to the Hankel functions. If we use only the first term in each asymptotic series, we obtain the not too surprising result

$$R = 0 \tag{B20}$$

We therefore retain two terms in the asymptotic expansion of each Hankel function. In the numerator and denominator of equation (B11) we retain terms up to first order in $1/\rho_0$ and $1/\rho_d$. The result is

$$R = \frac{1 - 2q}{4i\rho_0} + \frac{2q - 1}{4i\rho_d} \exp\left[2i(\rho_0 - \rho_d)\right]$$

$$= -\frac{am}{8ki}\left(1 - \frac{n_1}{n_2}\frac{e^{-i\omega T_D}}{1 + ad}\right) \tag{B21}$$

We have put in the definitions of q, ρ_0, and ρ_d, and T_D is the round trip transit time of a wave traveling across the transition region at the local phase velocity

$$T_D = 2\int_0^d \sqrt{\mu_0 \epsilon(z)}\,dz = \frac{2}{\omega}(\rho_d - \rho_0) \tag{B22}$$

In this calculation, R is referred to the point $z = 0$.

Now in equation (B21) there is a term with no time delay and one with time delay T_D. Thus, the reflected wave comes entirely from the points $z = 0$ and $z = d$. It is easily shown, moreover, that the amplitudes of the two reflections are proportional to the discontinuities in the slope of the impedance function ($\sqrt{\mu_0/\epsilon}$). If we carried our analysis to a higher order in $1/\rho_0$ and $1/\rho_d$, we would merely add in the effect of multiple reflections. There would be a term with time delay $2T_D$, one with $3T_D$, and so on. The reflections, in this case, clearly do not come from the transition region at all but from the two discontinuities.

The quantitative difference between the Epstein profiles and the discontinuous profiles can be seen by considering a sample calculation. Let L denote the distance required for a profile in dielectric constant to change from its initial value plus 10 percent to its initial value plus 90 percent of the total change, and choose an Epstein profile and a linear profile with the same L (fig. 12). A simple calculation shows that

$$d = 1.25\ L \tag{B23}$$

$$\sigma = 0.228\ L \tag{B24}$$

Reflection coefficients were calculated for a transition from $n = 1.0$ to $n = 1.1$ by

using equations (B4), (B11), and (B21). The transition length L was varied from 0 to 3.0 free space wavelengths. The results are shown in figure 14. The solid curve is for the Epstein profile, and the dashed curve is for the linear profile shown in figure 12. The dotted extension of the dashed curve shows the approximate result (eq. (B21)), where it differs appreciably from the exact result (eq. (B11)).

There are two interesting differences between the two curves of figure 14:

(1) The oscillatory character of the dashed curve denotes the interference effects due to reflections from the two boundaries.

(2) For large values of L/λ, the reflection coefficients calculated from the dashed curve would be much larger than those calculated by using the solid curve.

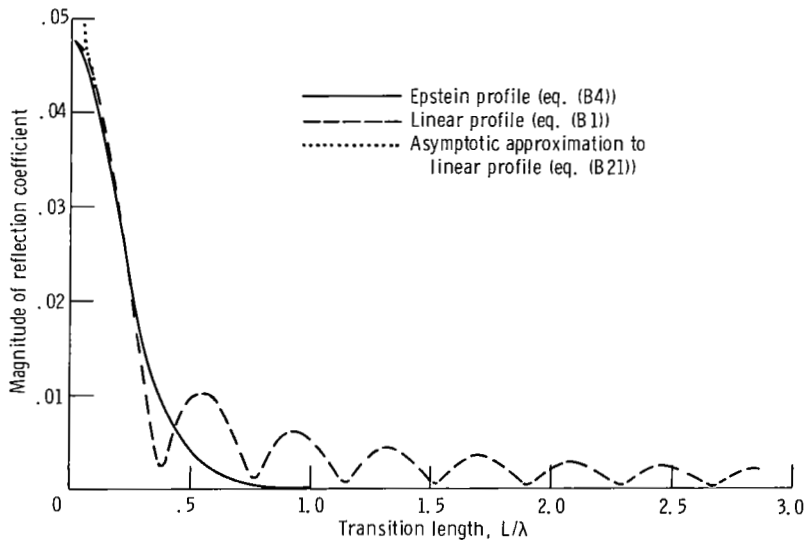

Figure 14. - Magnitude of reflection coefficient for Epstein profile and linear profile.

When the transition region is small compared to a wavelength, the difference between the different types of profile disappears. In the case shown, the solid and the dashed curves of figure 14 are in fair agreement as long as L/λ is less than about 0.25. (See also ref. 29.)

For gaseous plasmas, a continuous Epstein profile seems far more appropriate than profiles containing a discontinuity. This is true both in the laboratory (where a plasma sheath is formed at any plasma boundary) and in the ionosphere (where electron density and collision frequency changes must always be continuous, since there are no physical boundaries).

APPENDIX C

REFLECTION OF ELLIPTICALLY POLARIZED WAVES FROM A PLANE INTERFACE

The reflection coefficients of a plane interface between two regions of constant magnetoionic properties have been discussed in reference 11. Solutions are obtained for the case of linearly polarized and circularly polarized incident radiation. When a general elliptically polarized wave is incident on such a boundary, the situation is more complicated. The reflection and transmission coefficients can, however, be determined by consideration of the boundary conditions. Our formulation of the problem essentially follows that given in reference 17.

Consider a boundary plane between two regions of constant magnetoionic properties (fig. 15). Below the plane of incidence, the indices of refraction of the two modes are $n_a^{(1)}$ and $n_b^{(1)}$. The polarizations are $p_a^{(1)}$ and $p_b^{(1)}$; the subscripts "a" and "b" denote the two characteristic modes, ordinary and extraordinary. Above the boundary, we have $n_a^{(2)}$, $n_b^{(2)}$, $p_a^{(2)}$, $p_b^{(2)}$.

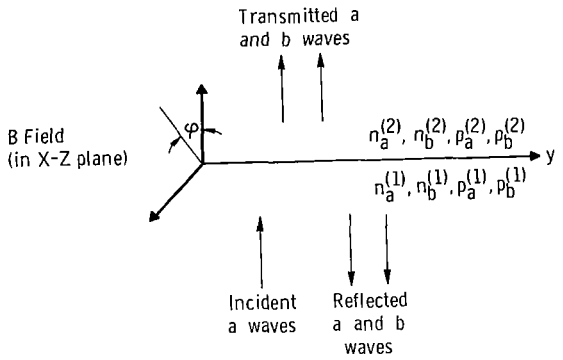

Figure 15. - Reflection from a plane interface.

Assume a type "a" wave incident from below ("a" may denote either ordinary or extraordinary). Assume also, for the time being, that there are reflected "a" and "b" waves and transmitted "a" and "b" waves. Our reflection and transmission coefficients R and T are defined in terms of the x component of the electric field. The first subscript on R and T specifies the incident wave and the second specifies the transmitted or reflected wave. The polarization for any wave is the ratio E_y/E_x for that wave in a right-hand coordinate system, with propagation in the Z direction and the magnetic field in the x-z plane (fig. 15). The wave polarizations obey the relation $p_a p_b = 1$ (ref. 11). The boundary conditions for E_x, E_y, H_y, and H_x give, respectively (ref. 17)

$$1 + R_{aa} + R_{ab} = T_{aa} + T_{ab} \tag{C1}$$

$$p_a^{(1)}(1 + R_{aa}) + p_b^{(1)}R_{ab} = p_a^{(2)}T_{aa} + p_b^{(2)}T_{ab} \tag{C2}$$

$$n_a^{(1)}(1 - R_{aa}) - n_b^{(1)}R_{ab} = n_a^{(2)}T_{aa} + n_b^{(2)}T_{ab} \tag{C3}$$

$$p_a^{(1)}n_a^{(1)}(1 - R_{aa}) - n_b^{(1)}p_b^{(1)}R_{ab} = n_a^{(2)}p_a^{(2)}T_{aa} + n_b^{(2)}p_b^{(2)}T_{ab} \tag{C4}$$

Before proceeding, let us delete all reference to the b wave to see when it is possible to obtain an uncoupled solution. Equations (C1) to (C4) become

$$1 + R_{aa} = T_{aa} \tag{C5}$$

$$p_a^{(1)}(1 + R_{aa}) = p_a^{(2)}T_{aa} \tag{C6}$$

$$n_a^{(1)}(1 - R_{aa}) = n_a^{(2)}T_{aa} \tag{C7}$$

$$n_a^{(1)}p_a^{(1)}(1 - R_{aa}) = n_a^{(2)}p_a^{(2)}T_{aa} \tag{C8}$$

Clearly, unless $p_a^{(1)} = p_a^{(2)}$, equations (C5) and (C6) are contradictory, as are equations (C7) and (C8). Only in the special cases of propagation along the magnetic field or normal to it will $p_a^{(1)} = p_a^{(2)}$. In the former case, $p = \pm i$ regardless of plasma properties. In the latter case, the two modes have $p = 0$ and $p = \infty$ for the ordinary and extraordinary modes, respectively.

For a general magnetoionic mode, then, the full forms of equations (C1) to (C4) are required. They can be conveniently written in matrix notation as

$$\begin{bmatrix} 1 & 1 & -1 & -1 \\ p_a^{(1)} & p_b^{(1)} & -p_a^{(2)} & -p_b^{(2)} \\ n_a^{(1)}p_a^{(1)} & n_b^{(1)}p_b^{(1)} & n_a^{(2)}p_a^{(2)} & n_b^{(2)}p_b^{(2)} \\ n_a^{(1)} & n_b^{(1)} & n_a^{(2)} & n_b^{(2)} \end{bmatrix} \begin{bmatrix} R_{aa} \\ R_{ab} \\ T_{aa} \\ T_{ab} \end{bmatrix} = \begin{bmatrix} -1 \\ -p_a^{(1)} \\ n_a^{(1)}p_a^{(1)} \\ n_a^{(1)} \end{bmatrix} \tag{C9}$$

or symbolically,

$$[M][R] = [P] \tag{C10}$$

Each matrix element in equation (C10) is a complicated function of plasma properties and wave frequency. In many cases, solutions are most easily obtained numerically, and this is the approach taken by Thrane (ref. 17). However, in the partial reflection experiments, the change in index of refraction at the reflecting interface is assumed small. In such a situation, equation (C10) should be solvable as a perturbation about the trivial case of no reflection. In the zero-order equation, we drop the change in plasma properties, so that $n^{(2)}_{a,b} = n^{(1)}_{a,b} = n_{a,b}$, and $p^{(2)}_{a,b} = p^{(1)}_{a,b} = p_{a,b}$. Then, clearly,

$$[M_0] = \begin{bmatrix} 1 & 1 & -1 & -1 \\ p_a & p_b & -p_a & -p_b \\ n_a p_a & n_b p_b & n_a p_a & n_b p_b \\ n_a & n_b & n_a & n_b \end{bmatrix} \tag{C11}$$

$$[R_0] = \begin{bmatrix} 0 \\ 0 \\ 1 \\ 0 \end{bmatrix} \tag{C12}$$

and

$$[P_0] = [P] = \begin{bmatrix} -1 \\ -p_a \\ n_a p_a \\ n_a \end{bmatrix} \tag{C13}$$

and the zero-order equation is

$$[M_0][R_0] = [P] \tag{C14}$$

It is easily seen that equation (C12) is a correct solution to equation (C14), since the vector [P] is identical to the third column of $[M_0]$. Now, referring to equation (C9), the components of [M] have terms up to second order in the perturbation quantities $\Delta n_{o,e}$

and $\Delta p_{o,e}$ ($\Delta n_{o,e} = n^{(2)}_{o,e} - n^{(1)}_{o,e}$, and $\Delta p_{o,e} = p^{(2)}_{o,e} - p^{(1)}_{o,e}$). The vector [P] has only zero-order components. A perturbation hierarchy can thus be established as follows:

$$[M_0][R_1] + [M_1][R_0] = 0 \tag{C15}$$

$$[M_0][R_k] + [M_1][R_{k-1}] + [M_2][R_{k-2}] = 0 \tag{C16}$$

where k is any order higher than one. Assuming that $[M_0]$ has an inverse,

$$[R_1] = -[M_0]^{-1}[M_1][R_0] \tag{C17}$$

$$[R_k] = -[M_0]^{-1}[M_1][R_{k-1}] - [M_0]^{-1}[M_2][R_{k-2}] \tag{C18}$$

It is easily shown by direct calculation that $[M_0]^{-1}$ is given by

$$[M_0]^{-1} = \frac{1}{2n_a n_b(p_b - p_a)} \begin{bmatrix} p_b n_a n_b & -n_a n_b & -n_b & n_b p_b \\ -p_a n_a n_b & n_a n_b & n_a & -n_a p_a \\ -p_b n_a n_b & n_a n_b & -n_b & n_b p_b \\ p_a n_a n_b & -n_a n_b & n_a & -n_a p_a \end{bmatrix} \tag{C19}$$

At any level of approximation, the result $[R_k]$ can be computed by matrix multiplication. The first-order result is probably adequate for our purposes and is given by

$$[R_1] = \begin{bmatrix} -\Delta n_a/2n_a \\ (n_b - n_a)\Delta p_a/2n_b(p_b - p_a) \\ -\Delta n_a/2n_a + \Delta p_a/2(p_b - p_a) \\ -(n_a + n_b)\Delta p_a/2n_b(p_b - p_a) \end{bmatrix} \tag{C20}$$

We are primarily interested in the first two components, R_{aa} and R_{ab}. To first order

$$R_{aa} = -\frac{\Delta n_a}{2n_a} \tag{C21}$$

$$R_{ab} = \frac{(n_b - n_a)\Delta p_a}{2n_b(p_b - p_a)} \tag{C22}$$

The first result (eq. (C21)) is quite reasonable, since it agrees with the Fresnel reflection formula when Δn_a is small. The second result (eq. (C22)) is very small, since it has the factor $(n_b - n_a)$ and both n_b and n_a are close to 1. We cannot rule out the possibility that a second order term without the factor $(n_b - n_a)$ would be comparable to equation (C22), even if $\Delta n_{a,b}$ and $\Delta p_{a,b}$ were small. We therefore calculate the second-order correction to equation (C22). Since the calculation is necessitated by the fact that n_a and n_b are close to unity, we set them equal to unity in the second-order correction. This eliminates a good deal of tedious work and does not, we believe, contribute appreciable errors to the result. In the interest of consistency, we also calculate the second-order correction to equation (C21) in the same way. The results are

$$R_{aa} \approx -\frac{\Delta n_a}{2n_a} + \frac{(\Delta n_a)^2}{4} \tag{C23}$$

$$R_{ab} \approx \frac{\Delta p_a}{2(p_b - p_a)}\left[\frac{(n_b - n_a)}{n_b} + \Delta(n_b - n_a)\right] \tag{C24}$$

Equations (C21) to (C24) are used to calculate values of R_{aa} and R_{ab} for a sample problem which was posed by Thrane (ref. 17). The results are shown in table I along with corresponding results obtained by Thrane using numerical solutions of the matrix equation. The plasma properties assumed in the calculation are reasonable for a height of 70 kilometers, which is near the center of the range in which partial reflection experiments are performed.

Values of n_a, n_b, p_a, and p_b were calculated by using the generalized magnetoionic theory of Sen and Wyller (ref. 14), with the subscript a assigned to the ordinary mode. The C script integrals in this theory were calculated by using the approximations given by Burke and Hara (ref. 15).

Table I shows that the first-order perturbation results for R_{aa} are in good agreement with the results given by Thrane (ref. 17). As expected, the second-order results for R_{aa} are not noticeably different from the first-order results. The results for the cross reflection coefficient R_{ab} are somewhat different. The first-order calculation agrees with the results of reference 17 only when $\Delta N/N$ and $\Delta\nu/\nu$ are small. When $\Delta N/N$ or $\Delta\nu/\nu$ equal unity, it is necessary to go to second order to get good agreement. The smallness of the cross reflection coefficient, either absolutely or compared

TABLE I. - REFLECTION COEFFICIENT R_{aa} AND CROSS-REFLECTION COEFFICIENT R_{ab} FOR SAMPLE PROBLEM FROM REFERENCE 17

[Gyrofrequency, 1.20 MHz; wave frequency, 2.3 MHz; dip angle, 50^{o}; electron number density, N, 200 per cm^{3}; collision frequency, ν, 4×10^{6} per sec.]

Relative change	Numerical results from reference 17	Results of perturbation method	
		First order	Second order
	Reflection coefficient, R_{aa}		
$\Delta N/N$ (with $\Delta\nu = 0$)			
0.01	4.81×10^{-6}	4.85×10^{-6}	4.85×10^{-6}
.10	4.81×10^{-5}	4.84×10^{-5}	4.84×10^{-5}
1.00	4.81×10^{-4}	4.85×10^{-4}	4.85×10^{-4}
$\Delta\nu/\nu$ (with $\Delta N = 0$)			
0.01	1.77×10^{-6}	1.79×10^{-6}	1.79×10^{-6}
.10	1.72×10^{-5}	1.74×10^{-5}	1.74×10^{-5}
1.00	1.34×10^{-4}	1.35×10^{-4}	1.35×10^{-4}
	Cross-reflection coefficient, R_{ab}		
$\Delta N/N$ (with $\Delta\nu = 0$)			
0.01	5×10^{-10}	5.32×10^{-10}	5.37×10^{-10}
.10	6×10^{-9}	5.36×10^{-9}	5.90×10^{-9}
1.00	1.0×10^{-7}	5.37×10^{-8}	1.08×10^{-7}
$\Delta\nu/\nu$ (with $\Delta N = 0$)			
0.01	6×10^{-8}	6.07×10^{-8}	6.03×10^{-8}
.10	5.4×10^{-7}	5.82×10^{-7}	5.46×10^{-7}
1.00	2.4×10^{-6}	4.30×10^{-6}	2.48×10^{-6}

to the direct reflection coefficient, is also apparent. At an altitude of 70 kilometers, the cross reflection coefficients are two to four orders of magnitude smaller than the related direct reflection coefficients.

REFERENCES

1. Gardner, F. F.; and Pawsey, J. L.: Study of the Ionospheric D-Region Using Partial Reflections. J. Atmos. Terr. Phys., vol. 3, no. 6, 1953, pp. 321-344.

2. Gregory, John B.: Radio Wave Reflections from the Mesosphere. 1. Heights of Occurrence. J. Geophys. Res., vol. 66, no. 2, Feb. 1961, pp. 429-445.

3. Belrose, J. S.; and Burke, M. J.: Study of the Lower Ionosphere Using Partial Reflections. 1. Experimental Technique and Method of Analysis. J. Geophys. Res., vol. 69, no. 13, July 1, 1964, pp. 2799-2818.

4. Thrane, E. V.; Haug, A.; Bjelland, B.; Anastassiades, M.; and Tsagakis, E.: Measurements of D-Region Electron Densities During the International Quiet Sun Years. J. Atmos. Terr. Phys., vol. 30, Jan. 1968, pp. 135-150.

5. Gregory, J. B.; and Manson, A. H.: Seasonal Variations of Electron Densities Below 100 km at Mid-Latitudes. - I. Differential Absorption Measurements. J. Atmos. Terr. Phys., vol. 31, May 1969, pp. 683-701.

6. Fejer, J. A.: The Absorption of Short Radio Waves in the Ionospheric D and E Regions. J. Atmos. Terr. Phys., vol. 23, 1961, pp. 260-274.

7. Belrose, J. S.; Bourne, I. A.; and Hewitt, L. W.: A Critical Review of the Partial Reflection Experiment. Proceedings of Conference on Ground Based Radio Wave Studies of the Lower Ionosphere, Defense Research Board, Ottawa, 1967, pp. 125-151.

8. Belrose, John S.: Radio Wave Probing of the Ionosphere by the Partial Reflection of Radio Waves (From Heights Below 100 km). J. Atmos. Terr. Phys., vol. 32, Apr. 1970, pp. 567-596.

9. Connolly, D. J.: Differential Phase Shift of Partially Reflected Radio Waves. Radio Sci., vol. 6, no. 8-9, Aug.-Sept. 1971, pp. 757-762.

10. von Biel, H. A.; Flood, W. A.; and Camnitz, H. G.: Differential-Phase Partial Reflection Technique For the Determination of D-Region Ionization. J. Geophys. Res., vol. 75, no. 25, Sept. 1, 1970, pp. 4863-4870.

11. Budden, K. G.: Radio Waves in the Ionosphere. Cambridge Univ. Press, 1961.

12. Austin, G. L.; and Manson, A. H.: On the Nature of the Irregularities That Produce Partial Reflections of Radio Waves From the Lower Ionosphere (70-100 km). Radio Sci., vol. 4, no. 1, Jan. 1969, pp. 35-40.

13. Manson, A. H.; Merry, M. W. J.; and Vincent, R. A.: Relationship Between the Partial Reflection Of Radio Waves From The Lower Ionosphere and Irregularities as Measured by Rocket Probes. Radio Sci., vol. 4, no. 10, Oct. 1969, pp. 955-958.

14. Sen, H. K.; and Wyller, A. A.: On the Generalization of the Appleton-Hartree Magnetoionic Formulas. J. Geophys. Res., vol. 65, no. 12, Dec. 1960, pp. 3931-3950.

15. Burke, M. J.; and Hara, E. H.: Tables of the Semiconductor Integrals Cp(x) and Their Approximations for Use With the Generalized Appleton-Hartree Magnetoionic Formulas. Rep. DRTE-1113, Defense Res. Telecommunications Establishment, Ottawa, Canada, 1966.

16. Thrane, E. V.; and Piggott, W. R.: The Collision Frequency in the E- and D-Regions of the Ionosphere. J. Atmos. Terr. Phys., vol. 28, Aug. 1966, pp. 721-737.

17. Thrane, E. V.: Experimental Studies of the Structure of the Ionospheric D-Region. NDRE-54, Norwegian Defense Research Establishment, Oct. 1966.

18. Clemmow, P. C.; and Heading, J.: Coupled Forms of the Differential Equations Governing Radio Propagation in the Ionosphere. Proc. Camb. Phil. Soc., vol. 50, pt. 2, Apr. 1954, pp. 319-333.

19. Booker, H. G.: A Theory of Scattering by Nonisotropic Irregularities With Application to Radar Reflections from the Aurora. J. Atmos. Terr. Phys., vol. 8, no. 4/5, 1956, pp. 204-221.

20. Flood, W. A.: Revised Theory For Partial Reflection D-Region Measurements. J. Geophys. Res., vol. 73, no. 17, Sept. 1, 1968, pp. 5585-5598.

21. Flood, Walter A.: Reply (to 0. Holt). J. Geophys. Res., vol. 72, no. 21, Oct. 1, 1969, pp. 5183-5186.

22. Bolgiano, R., Jr.: The General Theory of Turbulence (and) Turbulence in the Atmosphere Winds and Turbulence in Stratosphere, Mesosphere and Ionosphere. K. Rawer, ed., John Wiley & Sons, Inc., 1968.

23. Wallot, J.: Der Senkrechte Durchgang Elektro-Magnetischer Wellen Durch Eine Schicht Räumlich Veränderlicher Dielektri-itätskonstante. Ann. d. Physik, Ser. 8, vol. 60, Dec. 19, 1919, pp. 734-762.

24. Epstein, Paul S.: Reflection of Waves in an Inhomogeneous Absorbing Medium. Proc. Nat. Acad. Sci., vol. 16, no. 10, Oct. 15, 1930, pp. 627-637.

25. Albini, Frank A.; and Jahn, Robert G.: Reflection and Transmission of Electromagnetic Waves at Electron Density Gradients. J. Appl. Phys., vol. 32, no. 1, Jan. 1961, pp. 75-82.

26. Yen, K. T.: Microwave Reflection by Nonuniform Plasmas with Exponential Electron Distribution. J. Appl. Phys., vol. 35, no. 2, Feb. 1964, pp. 290-294.

27. Taylor, Leonard S.: Reflection of Electromagnetic Waves at Electron Density Ramps. J. Appl. Phys., vol. 32, no. 9, Sept. 1961, pp. 1796-1797.

28. Schelkunoff, S. A.: Remarks Concerning Wave Propagation in Stratified Media. Comm. Pure Appl. Math., vol. 4, no. 1, June 1951, pp. 117-128.

29. Yamada, R.: Reflection of Electromagnetic Waves From a Stratified Inhomogeneity. IRE Trans. on Antennas and Propagation, vol. AP-9, no. 4, July 1961, pp. 364-370.

NASA-Langley, 1972 —— 13 E-6701